

ELECTRON NUCLEAR DOUBLE RESONANCE OF THE BORON-VACANCY COMPLEX IN SILICON

M. Sprenger, R. van Kemp, E.G. Sieverts and C.A.J. Ammerlaan

Natuurkundig Laboratorium der Universiteit van Amsterdam,
Valckenierstraat 65, 1018 XE Amsterdam, The Netherlands

Abstract

After 1.5 MeV electron irradiation of boron doped silicon at $T=18$ K and subsequent anneal at $T=190$ K the electron paramagnetic resonance spectrum Si-G10 was observed. This spectrum has tentatively been identified with a boron-vacancy complex in triclinic symmetry by Watkins. In the present study we prove the presence of boron in the center with electron nuclear double resonance (ENDOR) measurements. The hyperfine and quadrupole interactions with both boron isotopes (^{10}B , natural abundance 18.8%, nuclear spin $I=3$ and ^{11}B , 81.2%, $I=3/2$) were determined as well as the nuclear g -values. The implications of these interaction parameters to the atomic model are discussed.

Introduction

The present study is concerned with a defect in low-temperature electron-irradiated silicon, identified as a boron-vacancy pair. In 1976, Watkins (1) found a new EPR-spectrum, labeled Si-G10, which he tentatively ascribed to a boron-vacancy pair. As he was unable to prove the presence of boron in the center, this identification was based upon circumstantial arguments and, more general, upon the knowledge of damage processes in low-temperature electron-irradiated silicon. The first low-temperature electron-irradiation experiments go back to 1963 (2), when Watkins found an EPR-spectrum (Si-G1) which he identified with the isolated lattice vacancy. Later, detailed models were proposed for the damage mechanisms in low-temperature irradiations (3). It was shown that, even at temperatures as low as 4 K, the silicon self-interstitial is highly mobile during the irradiations, whereas the vacancy is not. This makes the net damage production low because vacancy-interstitial pairs can recombine. In p-type material the production rate is higher as interstitials are captured in a very efficient way by the substitutional acceptor atoms, which become interstitial themselves (3), by a mechanism as:



where A stands for an acceptor atom, such as aluminum or boron. This model is further confirmed by the identification of two EPR spectra, Si-G18 and Si-G28, with Al_I (4) and B_I (5), respectively. At temperatures in the range of 160-180 K the vacancy in p-type silicon becomes mobile, which is reflected

in the formation of complexes such as divacancies and vacancy-impurity pairs. In aluminum doped material a spectrum with trigonal symmetry, Si-G9, was convincingly identified with a vacancy-aluminum complex with the aluminum atom on a nearest neighbor site of the vacancy, $V \cdot Al_S$ (6). This spectrum arises as well after a room-temperature irradiation of Al-doped silicon as after a low-temperature irradiation followed by an annealing step at $T=170$ K. The center disappears in the temperature range $200-250^\circ C$. Under similar conditions in B-doped material spectrum G10 arises. Although it has a lower symmetry than the G9 spectrum, a lower annealing temperature ($\sim 0^\circ C$) and no resolved B-hyperfine structure in EPR, Watkins concluded that the G10 spectrum must arise from a boron-vacancy pair. Because a nearest neighbor position is not likely in this low symmetry the boron atom has to be on a next nearest neighbor site of the vacancy. Figure 1 gives this atomic model in one of its 24 possible orientations.

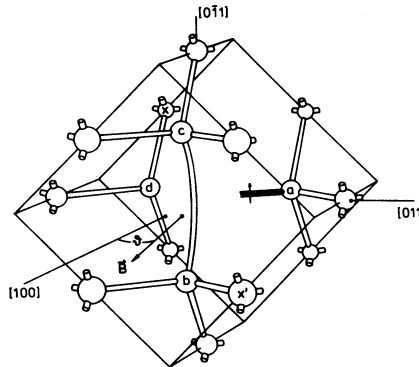


Figure 1 - Model of the boron-vacancy complex, after Watkins (1). The boron-atom is marked x, the orientation is dba.

In this paper we report electron nuclear double resonance (ENDOR) measurements on the Si-G10 spectrum, which beyond doubt prove the presence of one boron atom in the center. The next section gives information about the experimental procedure, then a summary of our experimental results is given followed by a discussion of the implications of our results to the defect model.

Experimental procedure

In a cryostat for combined low-temperature electron irradiation and spin resonance measurements we irradiated a sample of boron doped float-zone silicon (resistivity $0.1 \Omega cm$, $5 \times 10^{17} B.cm^{-3}$) with $1.5 MeV$ electrons to a fluence of $\sim 10^{17}$ electrons. cm^{-2} . During these irradiations the temperature was kept below $18 K$. The production of vacancies was monitored with the vacancy-associated EPR spectra Si-G1 and Si-G2. EPR and ENDOR measurements were performed using a superheterodyne spectrometer operating at a frequency of $23 GHz$. The magnetic field was rotated in the $(0\bar{1}1)$ -plane of the sample. Temperature could be varied during the measurements from $4 K$ to $30 K$. EPR spectra were recorded in dispersion mode with magnetic field modulation at a frequency of $83 Hz$ and phase sensitive detection. ENDOR was observed by extra square wave modulation of the RF-field at a frequency of $3.3 Hz$ and a second lock-in detector monitoring changes in the EPR-intensity. Best results for ENDOR of the Si-G10 spectrum were obtained at a temperature of $18 K$.

Experimental results

After anneal to a temperature of $190 K$ for 15 minutes we observed the EPR-spectrum G10. Figure 2a gives this EPR-spectrum in the three high-symmetry directions in the $(0\bar{1}1)$ -plane. The EPR measurements can be described with the spin-hamiltonian $H = \mu_B \vec{B} \cdot \vec{g} \cdot \vec{S}$ where \vec{S} is the electron-spin ($S=1/2$), \vec{B} is the magnetic field and \vec{g} is the g-tensor reflecting the

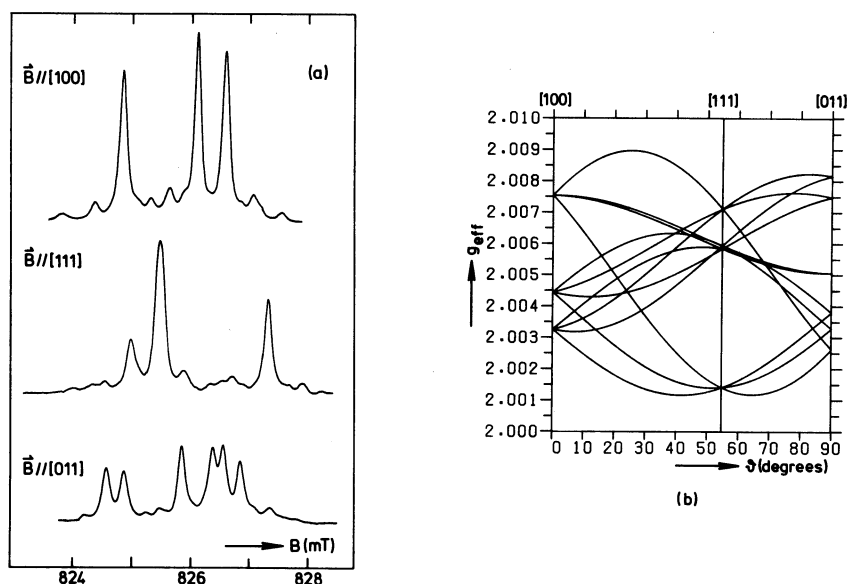


Figure 2 - EPR of the Si-G10 spectrum: (a) EPR spectra with the magnetic field in the three high-symmetry directions of the crystal at a temperature of 18K and with a microwave frequency of 23.176 GHz ; (b) angular dependence of the effective g-values as calculated from our least-squares fit for magnetic field directions in the (0T1)-plane. The 24 possible defect orientations coincide in pairs because the magnetic field is in this plane.

anisotropy of the defect. In this case the symmetry is low (triclinic), thus the symmetric g-tensor has 6 independent elements, i.e. there are no restrictions to the principal axes and principal values. The g-tensor elements were determined in a computer program with a least squares fit to the EPR data and found to be in close agreement with Watkins' values (1). Table I gives the principal values and principal axes of the g-tensor as found by us. Figure 2b shows the angular dependence of the g-values calculated with the fitted parameters. After warming up the sample to room-temperature the spectrum has disappeared, whereas the divacancy concentration, as monitored by the G6 spectrum, has grown appreciably.

In these EPR spectra clearly no trace of hyperfine interactions with the magnetic boron nuclei is found, apparently this interaction is too small to be observed as an EPR-splitting. In ENDOR experiments however, the resolving power is a few orders of magnitude larger than in EPR, because spectroscopically ENDOR is an NMR experiment. Figure 3 gives examples of ENDOR spectra from the high-field EPR line in the [100] direction (see figure 2a). These ENDOR spectra can be understood as arising from the ^{11}B and the ^{10}B nuclei respectively. The measurements must be described with a more complicated spin-hamiltonian, containing the boron nuclear spins:

$$\mathcal{H} = \mu_B \vec{s} \cdot \vec{g} \cdot \vec{s} - g_N \mu_N \vec{B} \cdot \vec{I} + \vec{s} \cdot \vec{A} \cdot \vec{I} + \vec{I} \cdot \vec{Q} \cdot \vec{I} \quad (2)$$

where \vec{s} is the electron spin ($S=1/2$), \vec{I} is the nuclear spin ($I=3$, ^{10}B , natural abundance 18.8% or $I=3/2$, ^{11}B , 81.2%). The first term, as before, represents the electronic zeeman interaction, the second term the isotropic

nuclear zeeman interaction. The third term is the interaction between the electron and nuclear spins, the hyperfine interaction, and the last term is the nuclear quadrupole interaction. The hyperfine interaction tensor \vec{A} has six independent elements in this symmetry, the quadrupole interaction tensor \vec{Q} , which is taken traceless, has five. Thus the total spin-hamiltonian of eq. 3 contains 18 independent parameters for each of the two possible nuclear spin values, the dimension is 14×14 in the case of ^{10}B and 8×8 in the case of ^{11}B . Figure 4 gives first order solutions for the eight energy levels in the simplest case, ^{11}B , $S=1/2$, $I=3/2$. This figure serves as an aid in understanding the possible transitions in this system. EPR transitions are those with $\Delta m_S = \pm 1$, $\Delta m_I = 0$, NMR transitions (seen in ENDOR) are those with $\Delta m_I = \pm 1$, $\Delta m_S = 0$. In this spectrum, as mentioned before, the splitting of the 4 EPR lines is too small compared to the EPR linewidth to be resolved. The six ENDOR lines however, are well separated, as shown in figure 3. Two groups of each three lines are visible, the two groups lying symmetrically around the nuclear zeeman frequency $\nu_z = g_N \mu_N B$. The splitting between the two groups is due to the hyperfine interaction, the splitting within the groups is due to the quadrupole interaction. In the ^{10}B case the situation is similar although the levelscheme contains 14 levels with 12 possible ENDOR transitions shown in figure 3. For $B=827 \text{ mT}$ the ^{10}B lines are found near 3.78 MHz, the ^{10}B nuclear zeeman frequency, and the ^{11}B lines near 11.3 MHz. Thus, the two isotopes can be treated separately in the analysis. In the high-symmetry directions slow scans were taken to get datapoints for a least-squares fit. From the angular dependence it was deduced which datapoints belong to which of the 12 possible orientations and then the parameters were fitted in a least squares program which fits the transitions to the eigenvalues of the hamiltonian matrices of dimension 8×8 and 14×14 respectively. As ENDOR transitions are to first order independent of the electronic g -values, during fitting of the ENDOR data the electronic g -value parameters were kept constant to the values previously found in the EPR fit. Thus here fits to 12 parameters were made. Table I gives the principal values and principal directions of the interaction tensors thus found; figure 5 shows the angular dependence of the hyperfine and quadrupole interactions in the case of ^{11}B . Because the hyperfine splitting is not resolved in EPR, it is not obvious to which EPR transition a certain NMR transition belongs, leaving an ambiguity in the sign of the quadrupole interaction with respect to the hyperfine interaction. By a special extension to the ENDOR technique, called Field Swept ENDOR (FSE), this ambiguity can be removed (8). The relative sign of the \vec{A} and \vec{Q} tensors as given in table I were determined with this technique (9). The electronic g -values, as mentioned before, are close to Watkins' values (1), the nuclear g -values are in turn close to those found in nuclear tables (7). The next section discusses the hyperfine and quadrupole parameters in view of the atomic model.

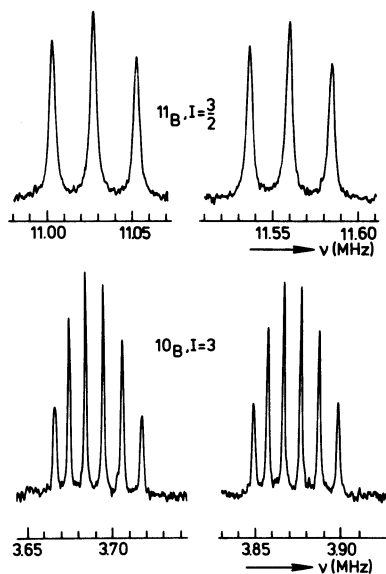


Figure 3 - ENDOR spectra of Si-G10 from the high-field EPR line, $B=826.73 \text{ mT}$, $\parallel [100]$.

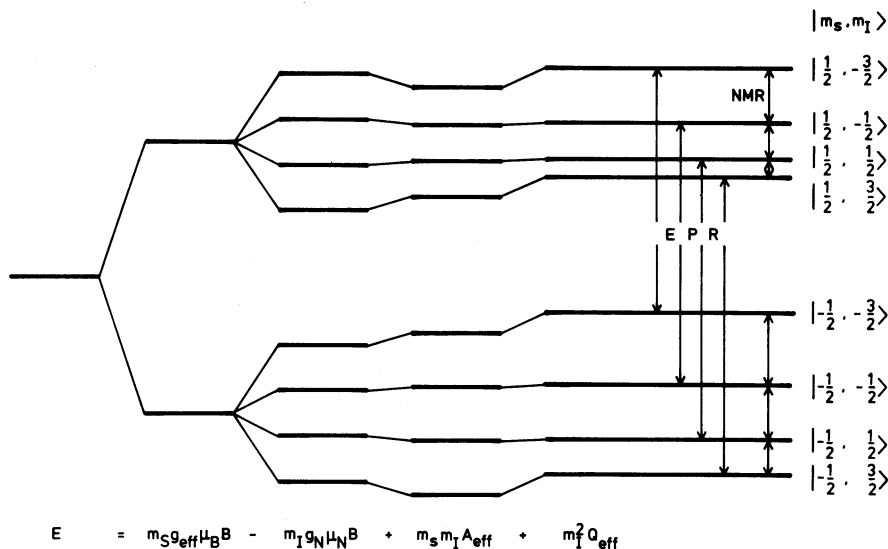


Figure 4 - Level scheme of the hamiltonian of eq. 2, for the case of ^{11}B ; the levels follow from first order solutions of the spin-hamiltonian. EPR and NMR transitions are indicated.

Discussion

The discussion on the experimental results will be divided into two parts, the hyperfine interactions and the quadrupole interactions. First, we will discuss the hyperfine interactions. It is usual to split hyperfine interaction tensors into two parts, $\vec{A} = a\vec{1} + \vec{B}$, where a is the isotropic part of the hyperfine tensor, $a = (\text{Tr}\vec{A})/3$, and \vec{B} is a symmetric, traceless tensor reflecting the anisotropic part of \vec{A} . Both parts have their interpretation in terms of wavefunctions, a is related to the wavefunction through the Fermi-contact interaction:

$$a = \frac{2}{3} \mu_0 g \mu_B g_N \mu_N |\Psi(0)|^2 \quad (3)$$

where $|\Psi(0)|^2$ is the probability density of the paramagnetic electron on the nucleus involved. The anisotropic part of the wavefunction arises from the spatial distribution of the wavefunction, the interaction involved is the dipole-dipole interaction between the magnetic moments of electron and nucleus. This tensor can be written as:

$$B_{ij} = \frac{\mu_0}{4\pi} g \mu_B g_N \mu_N \left\langle \Psi \left| \frac{3x_i x_j}{r^5} - \frac{\delta_{ij}}{r^3} \right| \Psi \right\rangle \quad (4)$$

where Ψ is the electronic wavefunction and $x_i, x_j = x, y, z$. As can be seen in eqs. 3 and 4 both parts of the hyperfine interaction scale with $g \mu_B g_N \mu_N$, thus, in the absence of any isotropic effect on the wavefunction one expects the ^{10}B and ^{11}B hyperfine parameters to be proportional to their g_N values. In table I one can see, that this is indeed the case. Therefore we will limit the discussion to follow to one of the two isotopes, ^{11}B .

When evaluating the figures of table I, one obtains a value of $a = -154.3$ kHz for the isotropic part of the hyperfine tensor and the values

Table I - Parameters of the spectrum Si-G10, determined by fitting the ENDOR data to the hamiltonian of eq. 2. The experimental error in the g-values is ± 0.0002 , units of the hyperfine and quadrupole parameters are kHz, the error is ± 0.5 kHz. The principal directions are for the orientation dba.

g-values	n[100]	n[010]	n[001]
$g_1=2.0090$	-0.8979	-0.3615	-0.2511
$g_2=2.0051$	0.1257	-0.7573	0.6408
$g_3=2.0011$	-0.4218	0.5439	0.7254

^{10}B				^{11}B			
$g_N=0.6002 \pm 0.0001$				$g_N=1.7921 \pm 0.0002$			
value(kHz)	n[100]	n[010]	n[001]	value(kHz)	n[100]	n[010]	n[001]
$A_1=180$	-0.788	-0.615	0.033	$A_1=537$	-0.792	-0.609	0.038
$A_2=-154$	-0.591	0.769	0.242	$A_2=-459$	-0.584	0.774	0.243
$A_3=-184$	-0.174	0.172	-0.970	$A_3=-541$	-0.177	0.170	-0.969
$Q_1=37$	0.636	0.661	0.398	$Q_1=88$	0.637	0.660	0.399
$Q_2=-11$	-0.361	-0.202	0.911	$Q_2=-26$	-0.361	-0.202	0.911
$Q_3=-26$	-0.682	0.723	-0.111	$Q_3=-62$	0.682	0.723	-0.110

$B_1=691.3$ kHz, $B_2=-304.7$ kHz and $B_3=-386.7$ kHz for the principal values of the anisotropic \vec{B} -tensor. These figures indicate a very small localization of the paramagnetic electron on the boron atom (one electron in a 2s orbital on the boron would give a value of $a=2.547$ GHz, ref(10)). Through the analysis of the resolved hyperfine structure with one ^{29}Si atom, Watkins (1) showed that 55% of the paramagnetic electron is concentrated in an orbital on one of the neighbors of the vacancy, the atom labeled a in figure 1. We will compare the anisotropic part of the boron hyperfine interaction tensor from our experiment with the hyperfine interaction due to dipole-dipole interaction of the boron nucleus with this electron. We assume a fraction of 55% of an electron being located as a point charge in the vacancy, the origin of figure 1. Such a dipole-dipole interaction yields a purely axial hyperfine tensor with principal values $2b, -b, -b$. Evaluation with eq. 4 gives the value of b:

$$b = \frac{\mu_0}{4\pi} g\mu_B g_N \mu_N \frac{1}{r^3} \quad (5)$$

The axial direction of this tensor is the connection between the two dipoles. Taking our experimental tensor axial for the moment, we have $b=345.7$ kHz, with the axial direction $[-0.792, -0.609, 0.038]$, only 7.7° from the $[\bar{1}\bar{1}0]$ direction, which is the direction where in Watkins' model the boron atom lies (in figure 1 the atom position marked x is on the $[\bar{2}\bar{2}0]$ -position). Calculation of b with eq. 5 gives $b=245.6$ kHz. We consider these results as a strong support for Watkins' atomic model, although the value of the calculated b is $\approx 30\%$ lower than the experimental value. Of course, in a more sophisticated treatment, one should take account of the fact, that the electron is not a point charge but spread out over a wavefunction. Furthermore a larger fraction than 55% will be located nearby the vacancy, in fact, ENDOR measurements reveal another 5% on each of the atoms b and c of figure 1 (9), which brings the total to 65%. Furthermore large distortions can occur around vacancies, and a distortion of only 10% of the Si-bond length is needed together with 65% of the electron as above to bring our point charge model in agreement with the experimental b-value. These models however do not give the absolute direction of the dipole-dipole axis, leaving the atom position at $[220]$, on the other side of the vacancy, equally probable. This position, marked x' in figure 1, is also allowed by Watkins' motional results (1).

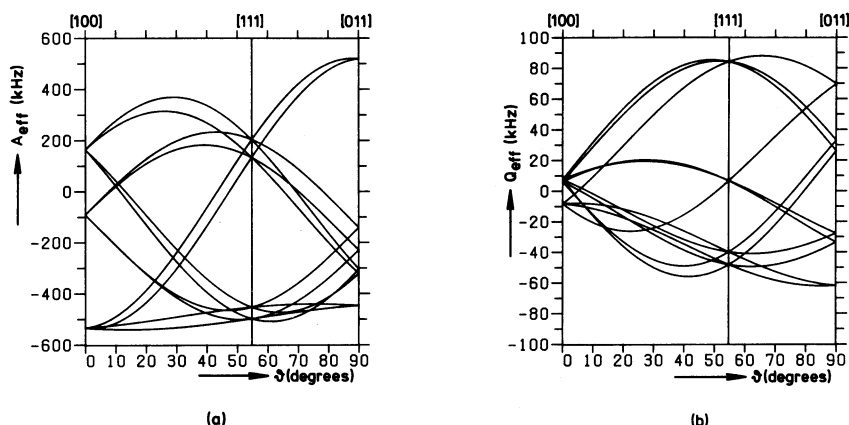


Figure 5 - Angular dependent patterns for ^{11}B calculated with the fitted hamiltonian parameters : (a) hyperfine interaction, (b) quadrupole interaction.

Now we will discuss briefly the quadrupole interaction, which can be described in terms of the interaction between the nuclear quadrupole moment and the electric field gradient at the nucleus:

$$Q_{ij} = \frac{eQ}{4I(2I-1)} \frac{\partial^2 V}{\partial x_i \partial x_j} \quad (6)$$

where e is the electron charge, Q is the nuclear quadrupole moment, I is the nuclear spin and V is the electrostatic potential (11). Thus, the \hat{Q} tensor is a measure of the total unbalanced charge density around the nucleus, and not only the spin density. It serves, like the hyperfine interaction, as a probe for the defect wavefunction, because the unperturbed crystal, with its cubic symmetry, does not contribute to these field gradients. The nuclear quadrupole moments can be found to be $8.5 \times 10^{-30} \text{ m}^2$ for ^{10}B and $4.1 \times 10^{-30} \text{ m}^2$ for ^{11}B (7). Again we can see from our measured values that there is no evidence of isotope shift on the electronic wavefunction. As in the case of the hyperfine interaction we will limit ourselves to the effects of an electronic point charge. Such a point charge at distance r yields an axially symmetric \hat{Q} tensor with principal values $2q, -q, -q$. With eq. 6 one can evaluate:

$$q = \frac{1}{4\pi\epsilon_0} \frac{e^2 Q}{4I(2I-1)} \frac{1}{r^3} \quad (7)$$

In the approximation of axial symmetry of the observed quadrupole interaction, with $q=44 \text{ kHz}$ for ^{11}B , and after substitution of the value for Q , we find one electron charge at a distance of about 0.6 Si-bond length. This value seems not unreasonable although detailed calculation in terms of electronic orbitals would be necessary to evaluate the experimental results completely. The axial direction of the \hat{Q} tensor, $[0.637, 0.660, 0.399]$, deviates only 11° from the $[111]$ direction. This slightly favors the atomic position x' in figure 1 over position x , because at x' the boron atom is in a $[111]$ direction with respect to one of the nearest neighbor atoms of the vacancy, labeled b in fig. 1, where such unbalanced charges may be expected.

Conclusions

In this work we have unambiguously proven the presence of one boron atom in the Si-G10 center. The boron hyperfine interaction tensor can be partly interpreted in terms of dipole-dipole interactions and serves as strong support for the atomic model. More detailed interpretation, also supported by ENDOR results for various silicon atoms around the complex, is left for the future.

References

- (1) G.D. Watkins, "EPR of a Trapped Vacancy in Boron-doped Silicon", *Phys. Rev.* **B13**, 2511 (1976).
- (2) G.D. Watkins, "An EPR Study of the Lattice Vacancy in Silicon", *J. Phys. Soc. Jap.* **18**, suppl II, 22 (1963).
- (3) G.D. Watkins, "EPR Studies of the Lattice Vacancy and Low-temperature Damage Processes in Silicon", in: *Lattice Defects in Semiconductors 1974*, edited by F.A. Huntley (The Institute of Physics, London, 1975), p1 ff.
- (4) G.D. Watkins, "A Review of EPR Studies in Irradiated Silicon", in: *Radiation Damage in Semiconductors*, edited by P. Baruch, (Dunod, Paris, 1965) p97 ff.
- (5) G.D. Watkins, "Defects in Irradiated Silicon: EPR and Electron Nuclear Double Resonance of Interstitial Boron", *Phys. Rev.* **B12**, 5824 (1975).
- (6) G.D. Watkins, "Defects in Irradiated Silicon: Electron Paramagnetic Resonance and Electron-Nuclear Double Resonance of the Aluminum-Vacancy Pair", *Phys. Rev.* **155**, 802 (1967).
- (7) G.H. Fuller, "Nuclear Spins and Moments", *J. Phys. Chem. Ref. Data* **5**, 835 (1976).
- (8) J.R. Niklas and J.M. Spaeth, "Application of ENDOR-Induced Electron Spin Resonance to the Study of Point Defects in Solids", *Phys. Status Solidi (b)* **101**, 221 (1980).
- (9) M. Sprenger et al, to be published.
- (10) J.R. Morton and K.F. Preston, "Atomic Parameters for Paramagnetic Resonance Data", *J. Magn. Reson.* **30**, 577 (1978).
- (11) T.P. Das and E.L. Hahn, "Nuclear Quadrupole Resonance Spectroscopy", *Solid State Phys., Suppl.* **1**, 1 (1958).